Biodegradation-affected fatigue behavior of extrusion-based additively manufactured porous iron–manganese scaffolds

Putra, Niko E.; Moosabeiki, Vahid; Leeflang, Marius A.; Zhou, Jie; Zadpoor, Amir A.

DOI
10.1016/j.actbio.2024.02.024

Publication date
2024

Document Version
Final published version

Published in
Acta Biomaterialia

Acta Biomaterialia 178 (2024) 340–351

Contents lists available at ScienceDirect

Acta Biomaterialia

journal homepage: www.elsevier.com/locate/actbio

Full length article

Biodegradation-affected fatigue behavior of extrusion-based additively manufactured porous iron–manganese scaffolds

Niko E. Putra*, Vahid Moosabeiki, Marius A. Leeflang, Jie Zhou, Amir A. Zadpoor

Department of Biomechanical Engineering, Faculty of Mechanical Engineering, Delft University of Technology, the Netherlands

ARTICLE INFO

Article history:
Received 29 November 2023
Revised 13 February 2024
Accepted 14 February 2024
Available online 21 February 2024

Keywords:
Additive manufacturing
Corrosion fatigue
Biodegradable metal
Porous material
Bone implant

ABSTRACT

Additively manufactured (AM) biodegradable porous iron-manganese (FeMn) alloys have recently been developed as promising bone-substituting biomaterials. However, their corrosion fatigue behavior has not yet been studied. Here, we present the first study on the corrosion fatigue behavior of an extrusion-based AM porous Fe35Mn alloy under cyclic loading in air and in the revised simulated body fluid (r-SBF), including the fatigue crack morphology and distribution in the porous structure. We hypothesized that the fatigue behavior of the architected AM Fe35Mn alloy would be strongly affected by the simultaneous biodegradation process. We defined the endurance limit as the maximum stress at which the scaffolds could undergo 3 million loading cycles without failure. The endurance limit of the scaffolds was determined to be 90 % of their yield strength in air, but only 60 % in r-SBF. No notable crack formation in the specimens tested in air was observed even after loading up to 90 % of their yield strength. As for the specimens tested in r-SBF, however, cracks formed in the specimens subjected to loads exceeding 60 % of their yield strength appeared to initiate on the periphery and propagate toward the internal struts. Altogether, the results show that the extrusion-based AM porous Fe35Mn alloy is capable of tolerating up to 60 % of its yield strength for up to 3 million cycles, which corresponds to 1.5 years of use of load-bearing implants subjected to repetitive gait cycles. The fatigue performance of the alloy thus further enhances its potential for trabecular bone substitution subjected to cyclic compressive loading.

Statement of significance

Fatigue behavior of extrusion-based AM porous Fe35Mn alloy scaffolds in air and revised simulated body fluid was studied. The Fe35Mn alloy scaffolds endured 90 % of their yield strength for up to 3×10^6 loading cycles in air. Moreover, the scaffolds tolerated 3×10^6 loading cycles at 60 % of their yield strength in revised simulated body fluid. The Fe35Mn alloy scaffolds exhibited a capacity of withstanding 1.5-year physiological loading when used as bone implants.

1. Introduction

Iron (Fe) and its alloys have in recent years been developed as a new category of biodegradable biomaterials for orthopedic applications [1]. Biodegradable porous bone implants are designed to degrade gradually in the body while promoting complete bone tissue regeneration. They are particularly suited for applications in which the implant functions temporarily in nature, such as bone fracture repair and bone defect reconstruction. The use of biodegradable (porous) implants significantly reduces the risk of adverse foreign body reactions that can occur when permanent implants are present in the body for a long period and eliminate the risk of long-term implant-associated infections [2].

The use of Fe-based biomaterials presents multiple challenges, including a low rate of biodegradation, MRI-incompatibility, and cytotoxicity [3]. In recent years, additive manufacturing (AM) has been used to address all these challenges. To address MRI-incompatibility and slow rate of biodegradation, both laser-based AM and extrusion-based AM have been utilized to create porous iron-manganese (FeMn) alloy scaffolds [4–6] that demonstrate paramagnetic properties and enhanced biodegradation rates while maintaining their stiffness at a level close to that of the native bone tissue. In a 48-week *in vivo* study, AM Fe30Mn scaffolds allowed for bony ingrowth and bone remodeling [7]. This find-

* Corresponding author.
E-mail address: n.e.putra@tudelft.nl (N.E. Putra).

https://doi.org/10.1016/j.actbio.2024.02.024

ing represents a significant advancement, as it contrasts to the findings of previous *in vivo* studies conducted on bulk Fe-based implants [8,9]. To address the potential cytotoxicity issue of Fe-based biomaterials, extrusion-based AM has been used to create the FeMn-bioceramic composites that show *in vitro* cytocompatibility towards preosteoblasts and promote the proliferation of the cells, their differentiation, and mineralization [10]. Thus, most of the challenges hampering the translation of iron-based biomaterials have already been addressed and the next steps need to be taken in this direction.

Load-bearing bone implants are designed to withstand million cycles of mechanical loading [11]. The translation of Fe-based biomaterials, therefore, requires data regarding their fatigue performance. The mechanical properties of FeMn porous implants reported in the literature exclusively concern their quasi-static compressive performances before and during *in vitro* biodegradation tests [4,5], and after *in vivo* tests at different time points with a small animal model [7]. The fatigue behavior of bone implants is influenced by multiple factors, such as the type and composition of the material, porosity, pore shape, pore size, overall topological design, surface features, and manufacturing processes that may induce defects or imperfections on the surfaces and in the interior, as well as residual stresses [12–14]. In the case of biodegradable implants, cyclic compressive loading affects the corrosion rate of the material. Conversely, the fatigue life of the material depends strongly on its corrosion behavior [15]. Most Fe-based biodegradable materials, developed so far, exhibit biodegradation rates lower than other biodegradable metals and alloys, such as Mg-based and Zn-based materials, and thus offer prolonged mechanical support at the bone defect site. Studying the corrosion fatigue behavior of Fe-based bone implants is, therefore, of particular importance. Up till now, the biodegradation-affected fatigue performances of AM biodegradable implants have only been evaluated for porous pure Fe [15], WE43 magnesium (Mg) alloy [16], pure zinc (Zn) [17], and Zn–3Mg alloy [18], all of which were fabricated through laser-based AM. There have been no reported studies on the biodegradation-affected fatigue behavior of extrusion-based AM biodegradable metals.

Here, we present the first ever study on the fatigue behavior of extrusion-based AM biodegradable porous bone implants. In particular, we studied the corrosion fatigue behavior of an extrusion-based AM porous FeMn alloy, containing 35 wt% Mn, intended for trabecular bone substitution. The chosen alloy was, in a previous study, demonstrated to be paramagnetic, and exhibited a favorable *in vitro* biodegradation rate and quasi-static compressive mechanical properties in the range of trabecular bone before and during *in vitro* biodegradation for 28 days in the revised-simulated body fluid (r-SBF) [5]. In this study, we tested the porous Fe35Mn alloy under compression-compression cyclic loading to simulate one of the main loading modes experienced by bone implants, *e.g.*, in the long bones or vertebral bones. Cyclic loading was applied in air and in a physiologically relevant condition: at 37 °C, 5 % CO_2 atmosphere, and in the r-SBF solution that has the same ion concentrations as the blood plasma [19].

2. Materials and methods

2.1. Fabrication of extrusion-based AM Fe-30Mn alloy scaffolds and post-processing

Porous Fe35Mn alloy scaffolds were designed to have a cylindrical shape, dimensions of Ø = 10 mm and h = 10.5 mm, and a layer-by-layer laydown pattern of 0° and 90° alternating angles.

Such geometrical pattern design has been reported to favor bone regeneration *in vivo* [20,21]. The strut size and strut spacing were respectively 410 µm and 400 µm. Fe powder (purity = 99.88 wt%, particle morphology = spherical, and particle sizes < 63 µm) and Mn powder (purity = 99.86 wt%, particle morphology = irregular, and particle sizes < 45 µm) were purchased from Material Technology Innovations Co. Ltd., China. The Fe and Mn powder mixture (with 35 wt% Mn) was blended with a 5 % hydroxypropyl methylcellulose solution (Sigma Aldrich, Germany) at the desired weight percentage (*i.e.*, 49.8 % powder ratio in the ink), as described in our previous publication [5]. Extrusion-based AM, more specifically direct ink writing of the Fe35Mn ink was performed using a 3D BioScaffolder 3.2 printer (GeSiM Bioinstruments and Microfluidics, Germany) with a nozzle size of 410 µm, at a printing pressure of 300 kPa and printing speed of 3.5 mm/s, and at room temperature, as described in our previous publication (Fig. 1a) [5]. After 3D printing, the Fe35Mn scaffolds were subjected heating at a rate of 2 °C/min to 350 °C for debinding for 3 h and then further heating at a rate of 8 °C/min to 1200 °C for sintering for 6 h in a tube furnace (STF16/180, Carbolite Gero Ltd., UK) under Ar flow (purity = 99.9999 %). The porous Fe35Mn specimens were then cleaned in isopropyl alcohol prior to corrosion fatigue tests, *in vitro* static immersion tests, and characterization.

2.2. Morphological characterization of the scaffolds

The morphological features of the specimens were observed using a scanning electron microscope (SEM, JSM-IT100, JEOL, Japan) and the chemical composition was determined by using an energy dispersive X-ray spectroscope (EDS, JSM-IT100, JEOL, Japan). The total porosity (ϕ) was calculated as:

$$\phi = \left(1 - \frac{m/\rho_{Fe35Mn}}{V_{bulk}}\right) \times 100\% \quad (1)$$

where m is the mass of the scaffold specimen (g) determined using a weighing scale of 0.1 mg accuracy, ρ is the density of the Fe35Mn alloy (7.63 g/cm^3 [22]), and V_{bulk} is the bulk volume of the cylindrical specimen (cm^3), calculated from the external diameter and height of the cylindrical specimen. The porosity in the strut of the scaffolds was visualized using microcomputed tomography (µCT) and scanning was performed using a Phoenix X-ray Nanotom® system (GE Sensing and Inspection Technologies GmbH, Germany). The micro-porosity of the struts was calculated using the BoneJ 7.0.17 plugin [23] (available in ImageJ, NIH, USA).

2.3. Fatigue tests in air and in revised simulated body fluid

Compression-compression cyclic loading was applied to the specimens by using a dynamic mechanical testing machine (Instron E10000 ElectroPuls with a 10 kN load cell) equipped with a double-wall specimen chamber designed and manufactured in-house (Fig. 1b). Four different maximum stress levels (*i.e.*, $0.6\sigma_y$, $0.7\sigma_y$, $0.8\sigma_y$, and $0.9\sigma_y$, where σ_y is the yield stress and equals 6.4 MPa) were applied at a frequency of 15 Hz. A loading ratio of 0.1 was used [15], meaning that the minimum stress level during each loading cycle was set to 0.1 time of the corresponding maximum stress level. The elastic modulus of the material prior to the fatigue tests was 0.39 GPa [5].

During the corrosion fatigue tests, the specimens were immersed in 300 mL r-SBF [19] inside the chamber. The temperature and pH were maintained at 37 °C and 7.40, respectively, while a mixture of 95 % N_2 and 5 % CO_2 was used as the purging gas flowing into the chamber to increase the buffering capacity. In addition, compression-compression cyclic loading was applied to another group of specimens in the ambient atmospheric condition (air) by using the same setup and mechanical testing machine under three different maximum stresses (*i.e.*, $0.6\sigma_y$, $0.8\sigma_y$, and $0.9\sigma_y$) using the same loading frequency and loading ratio.

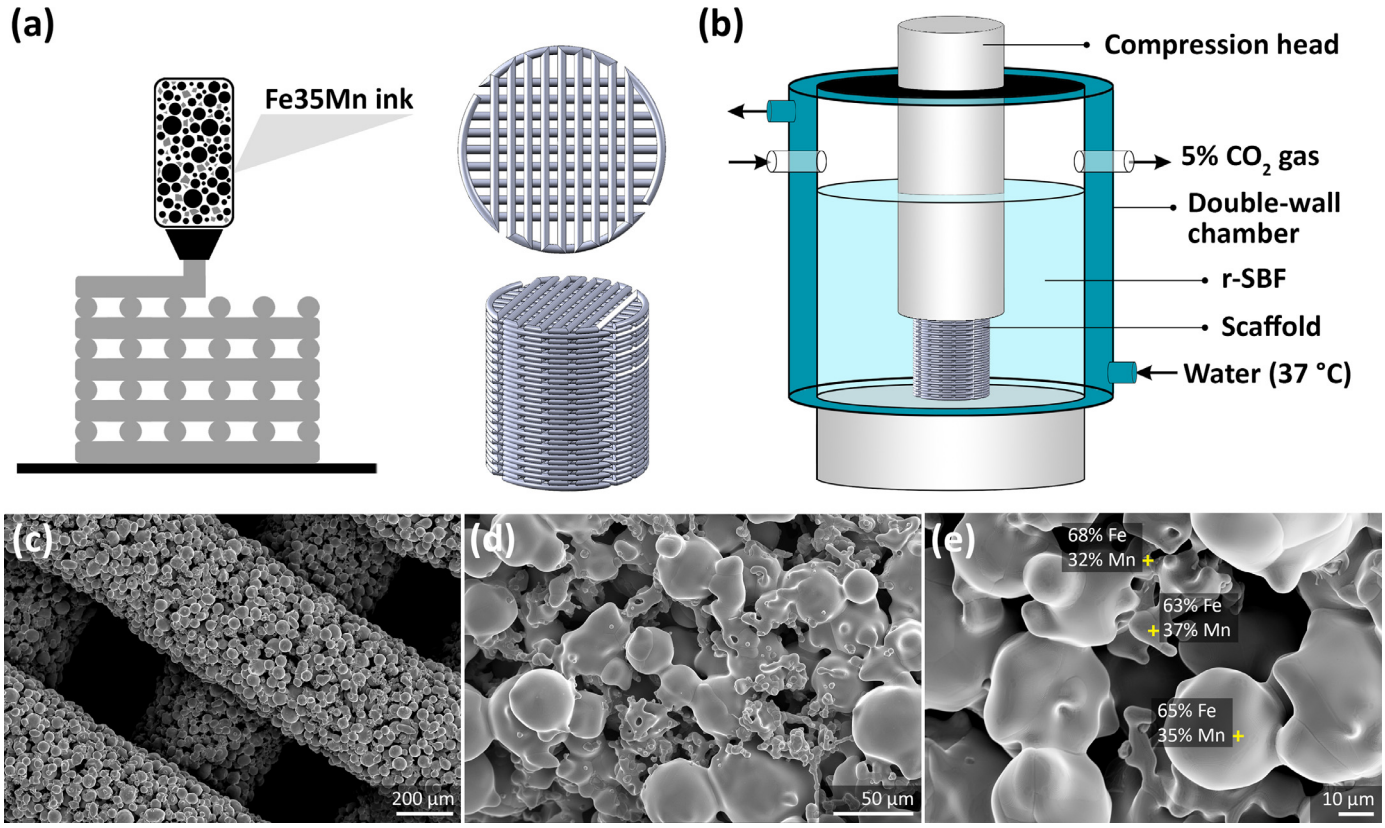

Fig. 1. (a) A schematic illustration of the extrusion-based AM for the Fe35Mn scaffolds with a laydown pattern of 0° and 90° alternating angles and the cylindrical design. (b) A schematic illustration of the corrosion fatigue test setup. The morphological and compositional features of the fabricated porous Fe35Mn scaffolds: (c) the as-sintered specimen containing macro-pores, (d) at a higher magnification, showing fused powder particles and the micro-pores interconnected into the struts, and (e) EDS analysis, indicating the chemical compositions at multiple spots.

All the tests were terminated either at a strain of 5 % (indicating specimen failure) or after 3 million cycles of loading (= 55.6 h). The tests were performed in triplicate for each stress level. The maximum stress value applied without causing specimen failure after 3 million cycles of loading was defined as the fatigue strength.

2.4. Static immersion tests in r-SBF

To separate the combined effects of biodegradation and cyclic loading, static immersion tests (regarded as the control groups) were performed in 300 mL r-SBF at 37 °C and under the atmospheric condition of 95 % N_2 and 5 % CO_2. The immersion time points were set in correspondence with those of the corrosion fatigue tests at four stress levels, *i.e.*, 55.6 h for $0.6\sigma_y$, 40 h for $0.7\sigma_y$, and 20.4 h for both $0.8\sigma_y$ and $0.9\sigma_y$. All the tests were performed in triplicate for each time point.

2.5. Measurement of ion release

The biodegradation rates of the specimens were determined by measuring the concentrations of Fe^{2+} and Mn^{2+} ions in r-SBF at different time points during corrosion fatigue tests and static immersion. During these tests, the concentrations of calcium (Ca^{2+}), and phosphate (PO_4^{3-}) ions in the r-SBF solution, in addition to those of Fe^{2+} and Mn^{2+}, were determined using an inductively coupled plasma optical emission spectroscope (ICP-OES, iCAP 6500 Duo, Thermo Scientific, USA). The Fe^{2+} and Mn^{2+} ion concentrations (in mg/L) measured after the corrosion fatigue and static immersion tests were normalized to the volume of the r-SBF solution and the immersion time.

2.6. Characterization of corrosion products and fatigue cracks

After the fatigue tests, the surface morphologies of the struts of the specimens subjected to cyclic loading in air and in r-SBF were observed using SEM (JSM-IT100, JEOL, Japan) at an accelerating voltage of 15 kV and a working distance of 10 mm. The chemical compositions of the corrosion products after the corrosion fatigue tests were analyzed using EDS combined with SEM (JSM-IT100, JEOL, Japan).

2.7. Characterization of fatigue crack morphology and distribution

The morphologies of the cracks at the periphery of the specimens after the corrosion fatigue tests were observed using SEM (JSM-IT100, JEOL, Japan). The specimens were cut horizontally to observe the morphologies of the cracks at the center. In addition, the initial specimens and the specimens subjected to cyclic loading at $0.8\sigma_y$ in combination with *in vitro* biodegradation were visualized using µCT (Phoenix X-ray Nanotom®, GE Sensing and Inspection Technologies GmbH, Germany). µCT was performed at a tube voltage of 120 kV, a tube current of 110 µA, a voxel size of 6 µm, a 360° rotation scan with an angular rotation of 0.25° each step, and a total duration of 60 min. Image analysis was performed using ImageJ (v1.54) (NIH, USA). µCT images were converted to 8-bit and the 3D model of the scaffolds was reconstructed using the 3D Slicer© software (v5.2.2, USA). Two different thresholds (*i.e.*, 125–135 and 135–255) were applied to segment the specimens with the

lower value to include the corrosion products and the higher value for the Fe35Mn alloy specimen only.

2.8. Statistical analysis

The differences in the concentrations of Fe^{2+}, Mn^{2+}, Ca^{2+}, and PO_4^{3-} ions during *in vitro* biodegradation with and without cyclic loading were analyzed using one-way ANOVA, followed by *post-hoc* Tukey test (**** = $p < 0.0001$, *** = $p < 0.001$, ** = $p < 0.01$, * = $p < 0.05$, and *n.s.* = not significant).

3. Results

3.1. Morphology and porosity of the AM Fe35Mn alloy scaffolds

The Fe35Mn alloy scaffolds exhibited a typical porous architecture commonly observed in extrusion-based AM specimens. The scaffolds featured a lay-down pattern with 90° angle switching between neighboring layers, as designed (Fig. 1c). The total porosity of the scaffolds was 68 ± 1 %. The struts of the scaffolds were porous and comprised of fused Fe and Mn powder particles (Fig. 1d). The micro-porosity within the struts, as determined by μCT, was 22 ± 2 %. The chemical compositions of the struts at multiple spots closely matched the intended chemical composition of the Fe and Mn elemental powder mixture prior to 3D printing as evidenced by the EDS spot analysis (Fig. 1e).

3.2. Fatigue behavior of the porous Fe35Mn alloy influenced by biodegradation

At the macroscale (Fig. 2a), no fracture plane was observed on the specimens after cyclic loading either in air or in r-SBF, even when the specimens failed (*e.g.*, at $0.8\sigma_y$ and $0.9\sigma_y$ in r-SBF). The specimens did not exhibit buckling, distortion, or slippage after cyclic loading under either of the environmental conditions. When tested in air, there were no apparent visual changes occurring to the specimens, while the specimens subjected to cyclic loading in combination with *in vitro* biodegradation were covered by corrosion products (Fig. 2a). The S-N curves indicated that the fatigue strength of the porous FeMn specimens (at 3 million cycles) decreased from $0.9\sigma_y$ in air to $0.6\sigma_y$ in r-SBF (Fig. 2b).

In air, all the specimens successfully endured the 3 million cycles of loading at the three chosen stress levels (Fig. 2c). Throughout the tests in air up to 3 million cycles, the specimens displayed a rapid increase in strain within the first 10 cycles (stage I) and then a further increase in strain within the first 100 cycles of loading (stage II), followed by a continued strain increase at a reduced rate towards 3 million cycles of loading (stage III). The accumulated strain value was lower under cyclic loading at a lower stress level (Fig. 2c). The specimens experienced an accumulated strain of 1.2 % under $0.9\sigma_y$ cyclic loading.

During the corrosion fatigue tests in r-SBF, the specimens survived 3 million cycles of loading at $0.6\sigma_y$ (Fig. 2c). However, the specimens failed earlier at 2.16 million cycles, 1.08 million cycles, and 1.13 million cycles when subjected to cyclic loading

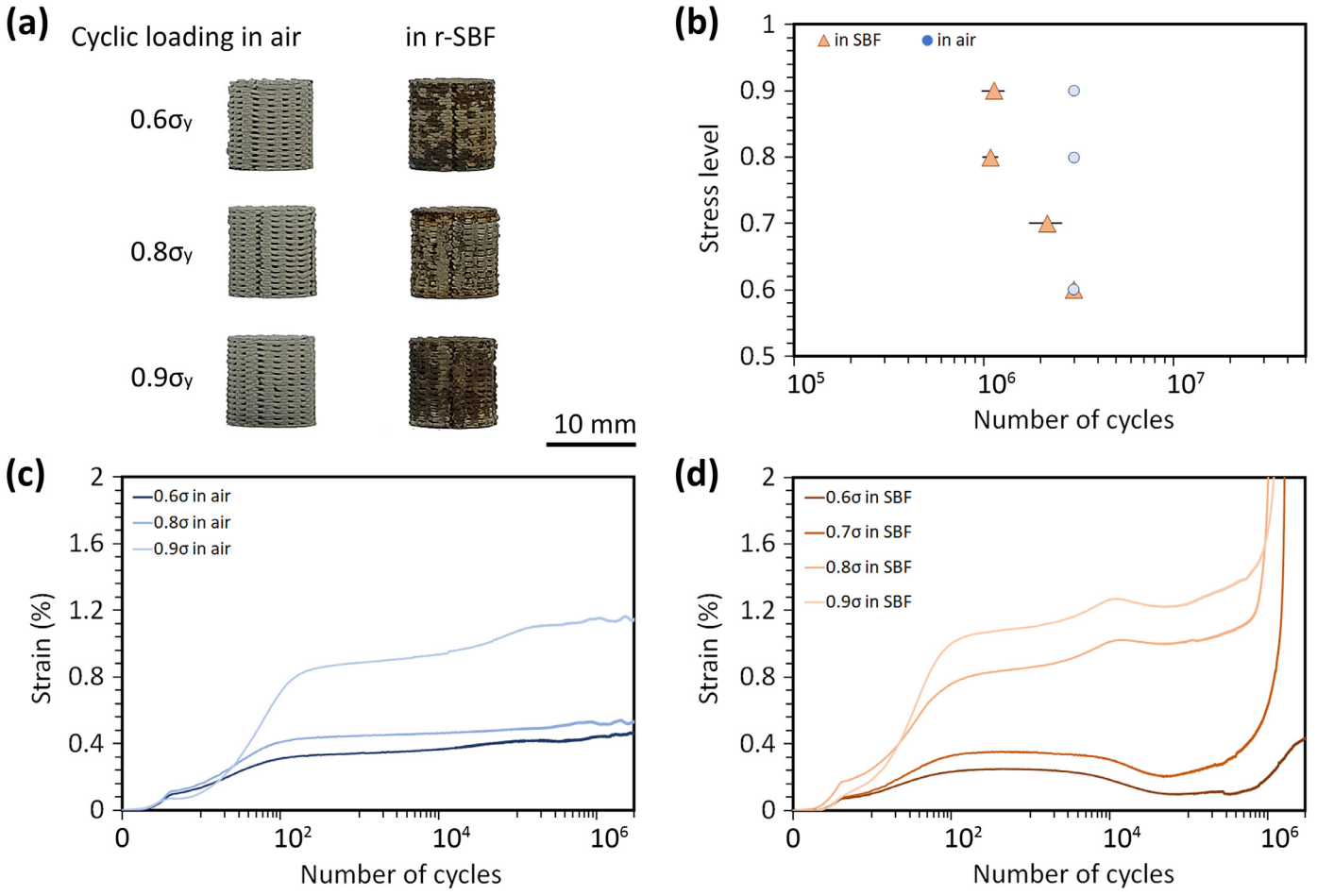

Fig. 2. The fatigue behavior of the extrusion-based AM Fe35Mn scaffolds: (a) the visual inspection of the specimens after cyclic loading at different stress levels in air and in r-SBF, (b) the S-N curve, (c) plots of strain *vs.* the number of loading cycles in air, and (d) the plots of strain *vs.* the number of loading cycles in r-SBF.

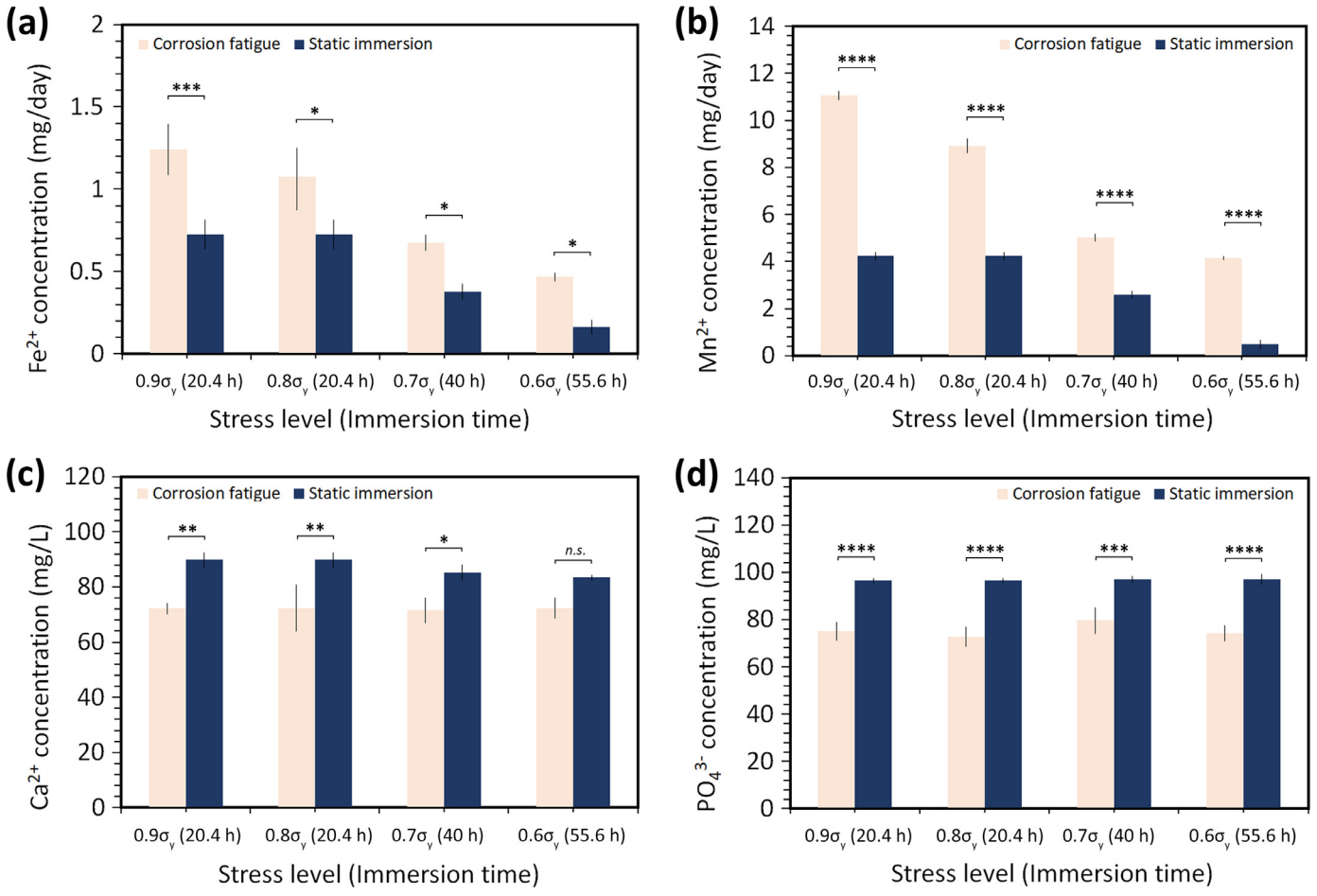

Fig. 3. (a) Fe^{2+}, (b) Mn^{2+}, (c) Ca^{2+}, and (d) PO_4^{3-} ion concentrations in r-SBF after the corrosion fatigue tests.

at higher stress levels, *i.e.*, 0.7σ_y, 0.8σ_y, and 0.9σ_y, respectively (Fig. 2b). Similar to the tests conducted in air, cyclic loading in r-SBF (Fig. 2d) resulted in a rapid increase in strain during the first 10 cycles (stage I), followed by a further increase in strain within the first 100 cycles of loading (stage II). After that, the strain value gradually increased at a reduced rate (stage III) until the specimen failed at a strain of 5 % or survived 3 million cycles of loading. Slight fluctuations in the strain accumulation trend were observed between $10^4$and 10^5 cycles (Fig. 2d).

3.3. Biodegradation behavior of the porous Fe35Mn alloy influenced by cyclic loading

Cyclic loading was found to enhance the biodegradation rate of the specimens, as compared to the biodegradation rate under the static immersion condition (Fig. 3a, and b). The biodegradation rate of the specimens was evaluated by comparing the concentrations of Fe^{2+} and Mn^{2+} ions in r-SBF. Cyclic loading at a higher stress level (*e.g.*, 0.9σ_y) led to higher ion concentrations of Fe^{2+} (Fig. 3a) and Mn^{2+} (Fig. 3b) in r-SBF, as compared to those at a lower stress level. The ion concentrations of Ca^{2+} (Fig. 3c) and PO_4^{3-} in r-SBF (Fig. 3d) were all lower when biodegradation occurred simultaneously with cyclic loading.

More corrosion products appeared on the specimens subjected to cyclic loading at a higher stress level (Fig. 4) in combination with *in vitro* biodegradation. EDS analysis revealed that all the corrosion products contained C, O, Na, Ca, Mn, and Fe (Table 1) without substantial differences. At the center of the specimens, some signs of localized corrosion (*e.g.*, pits) were observed on the surfaces of fused powder particles in the struts of the specimens subjected to cyclic loading at higher stress levels (*i.e.*, 0.8σ_y and 0.9σ_y, Fig. 5c–f).

3.4. Fatigue crack initiation and distribution

After cyclic loading in air at different loading levels, *i.e.*, at 0.6σ_y (Fig. 6a), 0.8σ_y (Fig. 6c), and 0.9σ_y (Fig. 6e), the struts of the specimens remained intact. At a higher magnification, no cracks were observed (Fig. 6b, d, and f). On the other hand, cracks were present to different extents on and even in all the specimens subjected to cyclic loading in r-SBF (Figs. 4 and 5). The struts of the specimens subjected to cyclic loading at 0.6σ_y for 3 million cycles of loading in r-SBF remained largely intact (Fig. 5a). Although the specimens did not fail after 3 million cycles of loading, some cracks on the peripheral struts had been initiated at the necks where the original powder particle were fused together (Fig. 4b). However, no cracks were found at the center of the specimens (Fig. 5a and b).

Under cyclic loading at higher stress levels (*i.e.*, at 0.8σ_y (Fig. 4c) and 0.9σ_y (Fig. 4e)) in r-SBF, wider and longer cracks were present on the struts of the specimens. On the periphery, cracks were found to occur at the necks of fused powder particles (Fig. 4d and f). Similar observations of fatigue cracks were made at the center of the specimens (Fig. 5c–f). More cracks had been initiated in the specimens subjected to cyclic loading at 0.8σ_y and 0.9σ_y in r-SBF as compared to those tested at 0.6σ_y.

The μCT images of the specimens subjected to the corrosion fatigue tests at 0.8σ_y showed a random distribution of cracks upon specimen failure (Fig. 7). Cracks were observed to occur mostly at

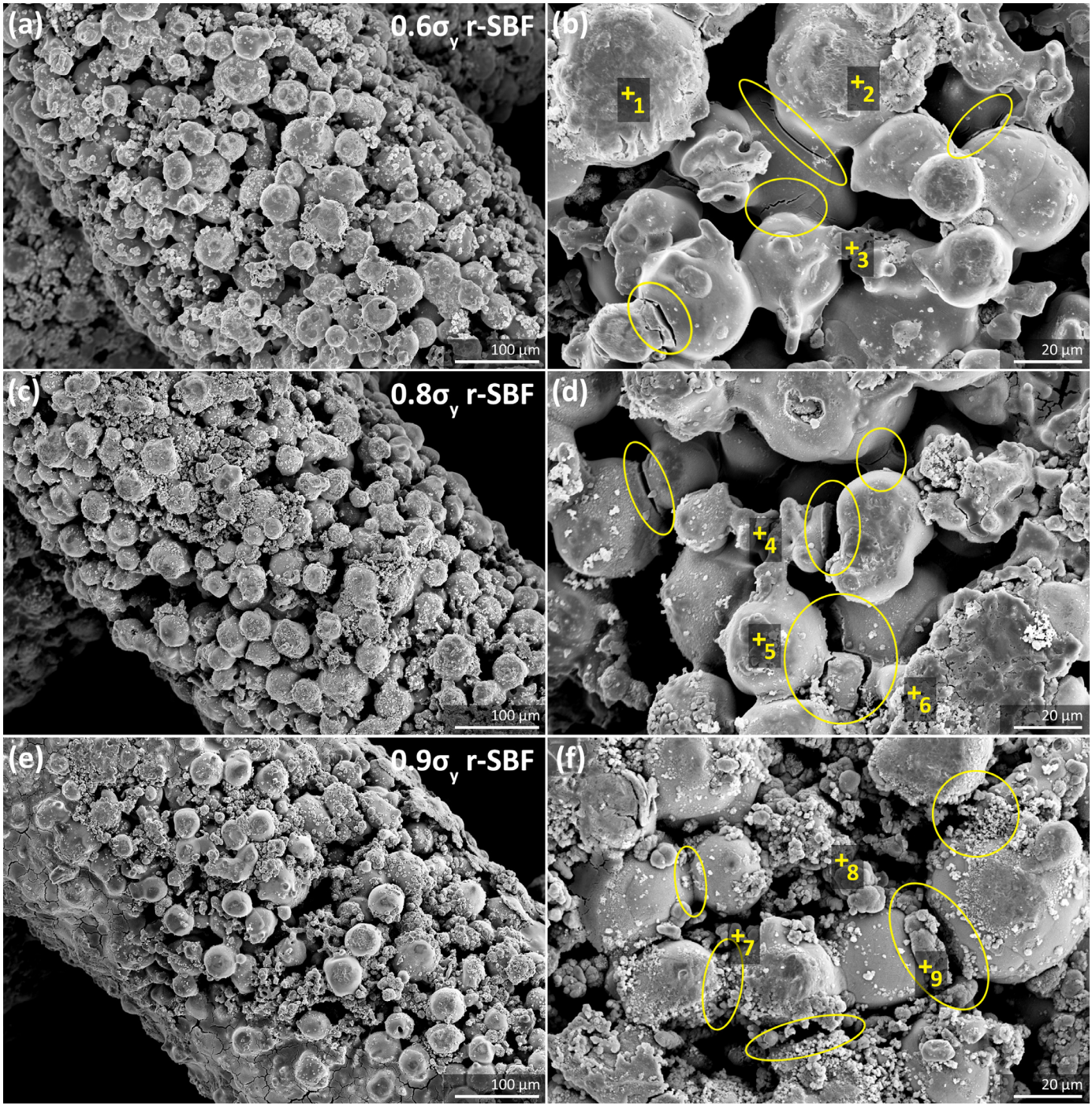

Fig. 4. Morphologies of the struts with fused FeMn powder particles, as well as the corrosion products on the periphery of the specimens after the corrosion fatigue tests at (a, b) $0.6\sigma_y$, (c, d) $0.8\sigma_y$, and (e, f) $0.9\sigma_y$. The cross marks indicate the spots of EDS analysis. The yellow ovals indicate the locations of fatigue cracks.

the junctions of struts between layers (Fig. 7a–c) and propagate almost through the entire strut (Fig. 7d–f). The 3D reconstruction of the specimens after the corrosion fatigue tests at $0.8\sigma_y$ for 10^4 cycles of loading and until specimen failure revealed the presence of corrosion products across the struts and in the micro-pores of the struts (Fig. 7g and h).

4. Discussion

There is currently a large knowledge gap regarding the corrosion fatigue performance of porous biodegradable alloys fabricated through extrusion-based AM. Here, we studied the fatigue behavior of the extrusion-based AM porous Fe35Mn alloy in air and in r-SBF to understand the mutual influences of cyclic loading and biodegradation on each other and to check if the biomaterial could withstand at least 1 million loading cycles [24], as required for bone implant applications. It was found that the porous Fe35Mn alloy, developed earlier, could indeed withstand 1 million cycles of loading at $0.9\sigma_y$, and at least 3 million cycles at $0.6\sigma_y$ in r-SBF, demonstrating its potential as a fatigue-resistant porous biodegradable implant material for trabecular bone substitution subjected to compressive cyclic loading, *e.g.*, in human vertebrae or greater trochanter of the femur [25,26]. It is, however, important to be aware that the results reported here

Table 1
The chemical compositions of the biodegradation products found on the struts of the Fe35Mn alloy scaffolds after the fatigue tests in r-SBF at different stress levels, as determined by EDS analysis (with an accuracy of 2 %).

EDS spot		C	O	Na	Ca	Mn	Fe
0.6σ_y in r-SBF	**1**	4.16	-	-	-	30.49	65.34
	2	4.82	15.31	4.66	0.78	57.85	16.58
	3	9.51	23.38	5.41	1.63	44.74	15.33
0.8σ_y in r-SBF	**4**	7.21	18.66	2.30	2.52	51.57	17.74
	5	13.75	10.14	-	0.50	55.27	20.34
	6	3.63	7.15	3.15	3.41	62.81	19.85
0.9σ_y in r-SBF	**7**	4.55	17.66	1.36	3.58	35.53	37.31
	8	8.94	31.55	2.51	2.53	32.05	22.41
	9	7.90	19.55	2.64	2.59	40.21	27.11

mark the very first step in the complex and lengthy trajectory of developing a bone-substituting material towards to its clinical adoption.

4.1. Microstructural features and fatigue behavior

The microarchitectural features of extrusion-based AM scaffolds, *e.g.*, diffusion bonding of the original powder particles as a result of solid-state sintering, porosity, pore sizes, and pore distribution, all affect their fatigue endurance. The porous Fe35Mn alloy scaffolds were designed with a 0° and 90° alternating pattern to have 90° interconnections between the struts. These scaffolds had macro-pores that were the spacing between the struts and interconnected micro-pores distributed inside the struts. This topological design is quite different from the typical laser-based AM specimens where the struts are designed to be nearly solid with minimal to no internal micro-pores. While micro-pores are generally considered to be stress concentrators, detrimental to fatigue strength [27], our findings suggest that these micro-pores are not detrimental as perceived.

The extrusion-based AM porous Fe35Mn alloy scaffolds, containing a relatively high micro-porosity in the struts (*i.e.*, 22 %), resisted at least 3 million cycles of loading at 0.9σ_y in air. This normalized fatigue strength is even higher than the normalized fatigue strength values of laser-based AM porous pure Fe [15] and Zn [17] scaffolds with solid struts and diamond unit cells (*i.e.*, at 0.7σ_y). There are different explanations for this unexpected advantage of extrusion-based AM over laser-based AM in terms of the fatigue behavior. First, it may be the case that while laser-based AM is successful in creating lattice structures with high quasi-static mechanical properties, these relatively high quasi-static mechanical properties cannot be maintained under cycling loading due to the much stronger effects of imperfections on the fatigue behavior under such high levels of mechanical loading. Second, it can be hypothesized that homogenous interconnected micro-pores may be of help in distributing stresses across the material, as compared to localized, clustered micro-pores [28]. This hypothesis is supported by a recent study on the fatigue behavior of porous titanium scaffolds with hierarchical porosity produced by using extrusion-based AM. It showed that the scaffolds with a higher internal micro-porosity (*i.e.*, 14.3 % *versus* 5.9 %) exhibited a higher fatigue endurance [29]. The authors attributed this observation to fatigue crack growth shielding effects occurring in such materials [29]. Similarly, the presence of internal pore defects in auxetic scaffolds made by laser-based AM was found to be not directly correlated with a significant decrease in fatigue strength [30]. It is however important to note that the role of micro-pores in influencing the corrosion fatigue behavior of biodegradable porous materials is much more complicated. Separate research dedicated to clarifying this role is needed.

While osteocytes can sense mechanical stimuli (*i.e.*, small strains), offering a potential avenue to promote bone health [31], the design of bone-mimetic scaffolds, including an optimum range of pore sizes, pore distribution, and total porosity, can provide adequate space for healthy bone regeneration [32,33]. In general, macro-pores enable bone ingrowth, while micro-pores improve cell adhesion [34]. For biodegradable metals, especially Fe-based alloys, open porosity is of great importance to provide a large, exposed surface area for biocorrosion to proceed. In addition to interconnected micro-pores within the struts, high roughness is another typical feature resulting from extrusion-based AM [35]. The influence of surface roughness on fatigue crack initiation and propagations has been extensively studied. A rough surface is generally considered an inherent imperfection of 3D printed products, detrimental to fatigue endurance [36,37]. However, average surface roughness may not correlate well with fatigue life [38]. Since the surface roughness of porous bony implants can improve osseointegration [39,40] and even possibly provide antibacterial properties [41], it is essential to reach an optimum balance, especially for biodegradable metals whose surface features change over time during biodegradation. In this connection, the exact influence of surface roughness on the corrosion fatigue behavior of biodegradable porous metals along with temporary changing surface features must be well understood through dedicated research.

4.2. Biodegradation-affected fatigue behavior

Under cyclic loading combined with biodegradation, the fatigue strength of the extrusion-based AM porous Fe35Mn scaffolds at 3 million cycles decreased from 0.9σ_y to 0.6σ_y. The relative magnitude of this reduction is larger than the one found in the corrosion fatigue tests of laser-based AM porous pure Fe scaffolds (from 0.7σ_y to 0.65σ_y) [15], although the trend is similar. The stronger influence of biodegradation on the fatigue strength of the porous Fe35Mn alloy can be explained by the higher micro-porosity in the struts and the higher corrosion rate of the Fe35Mn alloy as compared to pure Fe [5,42]. It is important to note that the fatigue strength of the porous Fe35Mn alloy is much higher than the fatigue strength of the porous WE43 Mg alloy (*i.e.*, 0.3σ_y in air and decreased to 0.2σ_y in r-SBF [16]), and the effect of biodegradation and corrosion products is totally different, when compared to porous Zn (*i.e.*, its fatigue strength being 0.7σ_y in air and 0.8σ_y in r-SBF) [17]. The fatigue strength of the AM porous Fe35Mn alloy (*i.e.*, 1 million cycles at 0.8–0.9σ_y in r-SBF) is superior to the fatigue strengths of porous Ti6Al4V alloy (*i.e.*, 1 million cycles at 0.5–0.55σ_y) [43] and the direct-ink-writing porous Ti6Al4V alloy

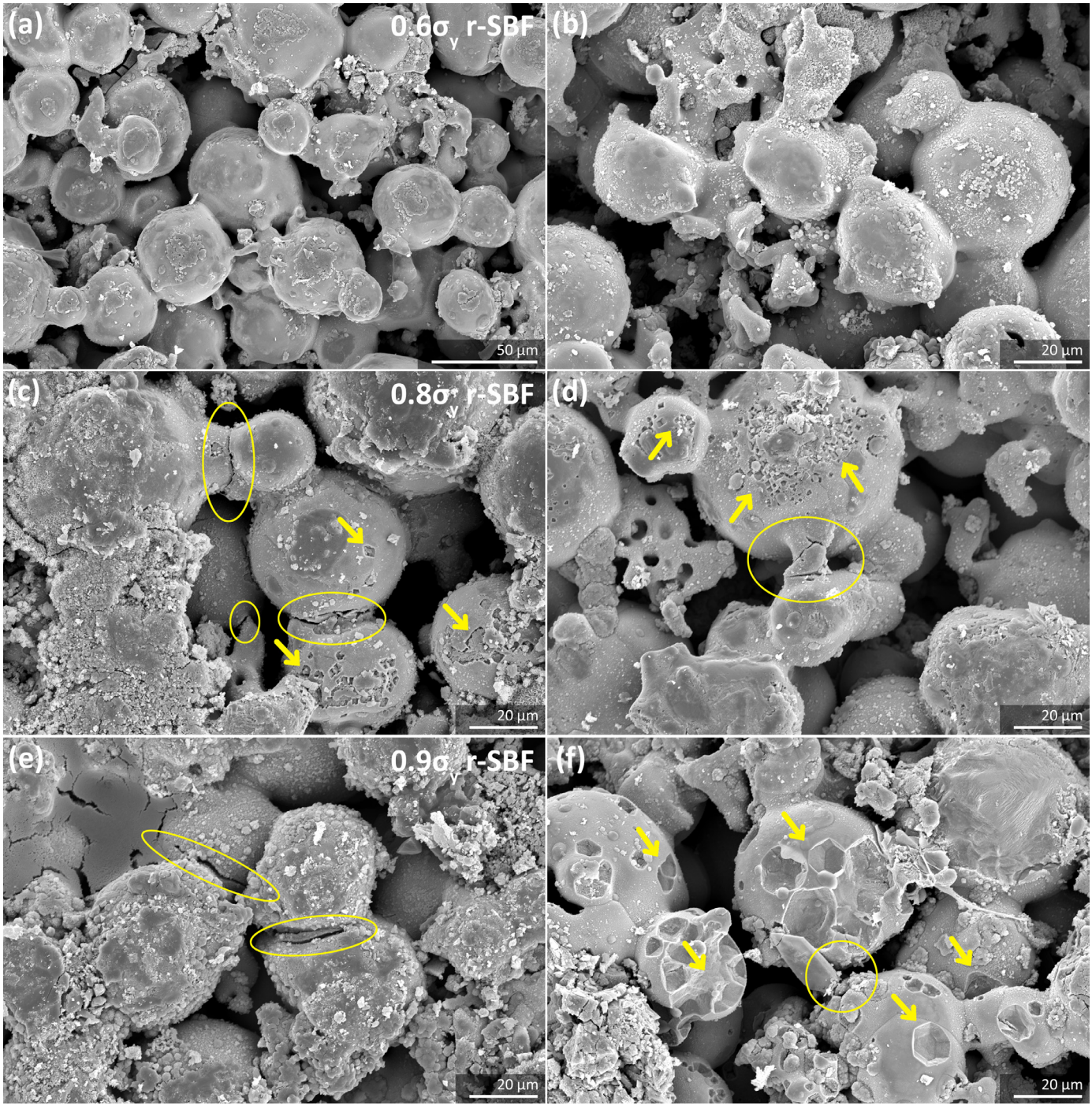

Fig. 5. The morphologies of the struts with fused FeMn powder particles as well as the corrosion products at the center of the specimens after the corrosion fatigue tests at (a, b) $0.6\sigma_y$, (c, d) $0.8\sigma_y$, and (e, f) $0.9\sigma_y$. The arrows indicate localized corrosion on the surface of the struts. The yellow ovals indicate the locations of cracks.

(*i.e.*, 1 million cycles at $0.62\sigma_y$) [29]. The fatigue endurance of the AM porous Fe35Mn alloy can be considered comparable to those of biomedical implants and human bone that are often evaluated up to 1 million cycles [44–46].

A biodegradable material for temporary bone substitution should withstand at least 1 million loading cycles without failure. The required endurance limit is determined, based on the average walking activity of a patient, equaling 2 million cycles per year, and on a bone fracture healing time of 21–24 weeks [47,48]. As the bone regenerates, the ingrowth of new tissue will strengthen the remaining implant and increase its fatigue endurance [49]. As presented earlier, the extrusion-based AM Fe35Mn alloy can withstand at least 1 million cycles of compressive loading at $0.8\sigma_y$ and $0.9\sigma_y$ in r-SBF (Fig. 2b). It is, therefore, expected to be able to meet the biomechanical requirements for trabecular bone substitution subjected to compressive loading, *e.g.*, in human vertebrae or greater trochanter part of the femur [25,26]. The number of loading cycles used in this study for determining the endurance limit of the AM materials developed is 3 million loading cycles, which, based on 2 million walking steps per year, equals an endurance corresponding to 1.5 years of service.

We studied the compression-compression corrosion fatigue behavior of the AM Fe35Mn scaffolds in the present research. It is however important to realize that the actual loading conditions

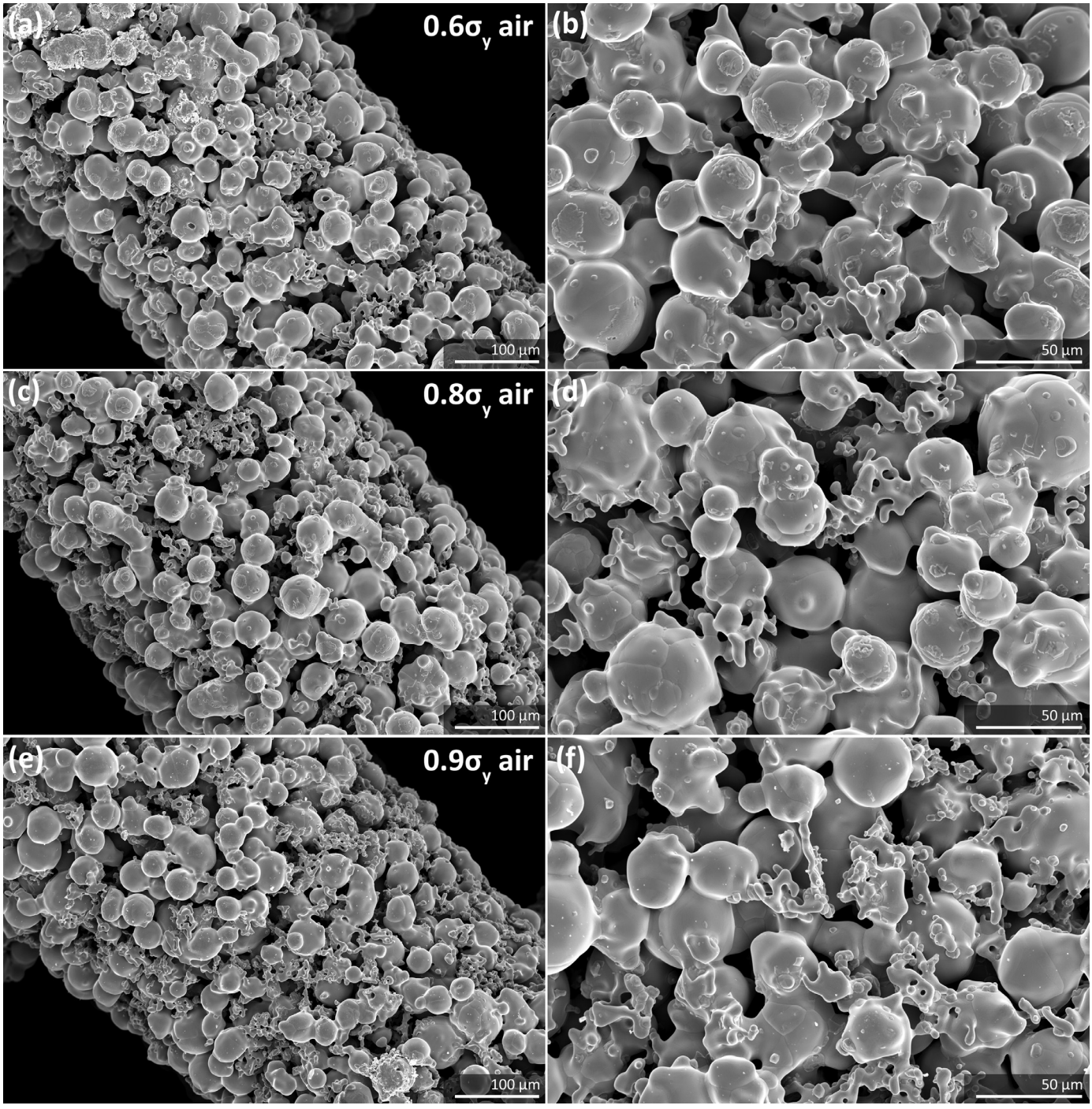

Fig. 6. Morphologies of the structs with fused FeMn powder particles on the periphery of the specimens after the fatigue tests in air at (a, b) $0.6\sigma_y$, (c, d) $0.8\sigma_y$, and (e, f) $0.9\sigma_y$.

may be different, depending on the implantation site as well as the specific type of implant for which the biomaterial is used. In other words, the porous Fe35Mn alloy developed in the previous study [5] and further investigated in this study may not be suitable for substituting the bone tissue subjected to cyclic loading where tensile or bending stresses are dominant. Separate research dedicated to studying the multi-axial mechanical performance of the material of varied architectural designs and the biomechanical performance *ex vivo* and *in vivo* are needed. In the meantime, it is also important to keep in mind that the fatigue behavior of AM porous biomaterials may be strongly dependent on the level of bony ingrowth and fatigue life may increase by up to 7 times under optimal bony ingrowth conditions [49]. Given that our experiments neglected the effect of bony ingrowth on simultaneously changing fatigue strength, the fatigue life obtained during these tests may be considered an underestimation of the fatigue life of porous implants where significant bony ingrowth takes place.

The measurement of strain accumulation is of use in understanding the underlying fatigue behavior, especially for porous materials, because damage to the porous structure due to (corrosion) fatigue is correlated to cumulative deformation [50,51]. The plots of strain against the number of loading cycles typically show three stages that are characteristic of the fatigue behavior of porous

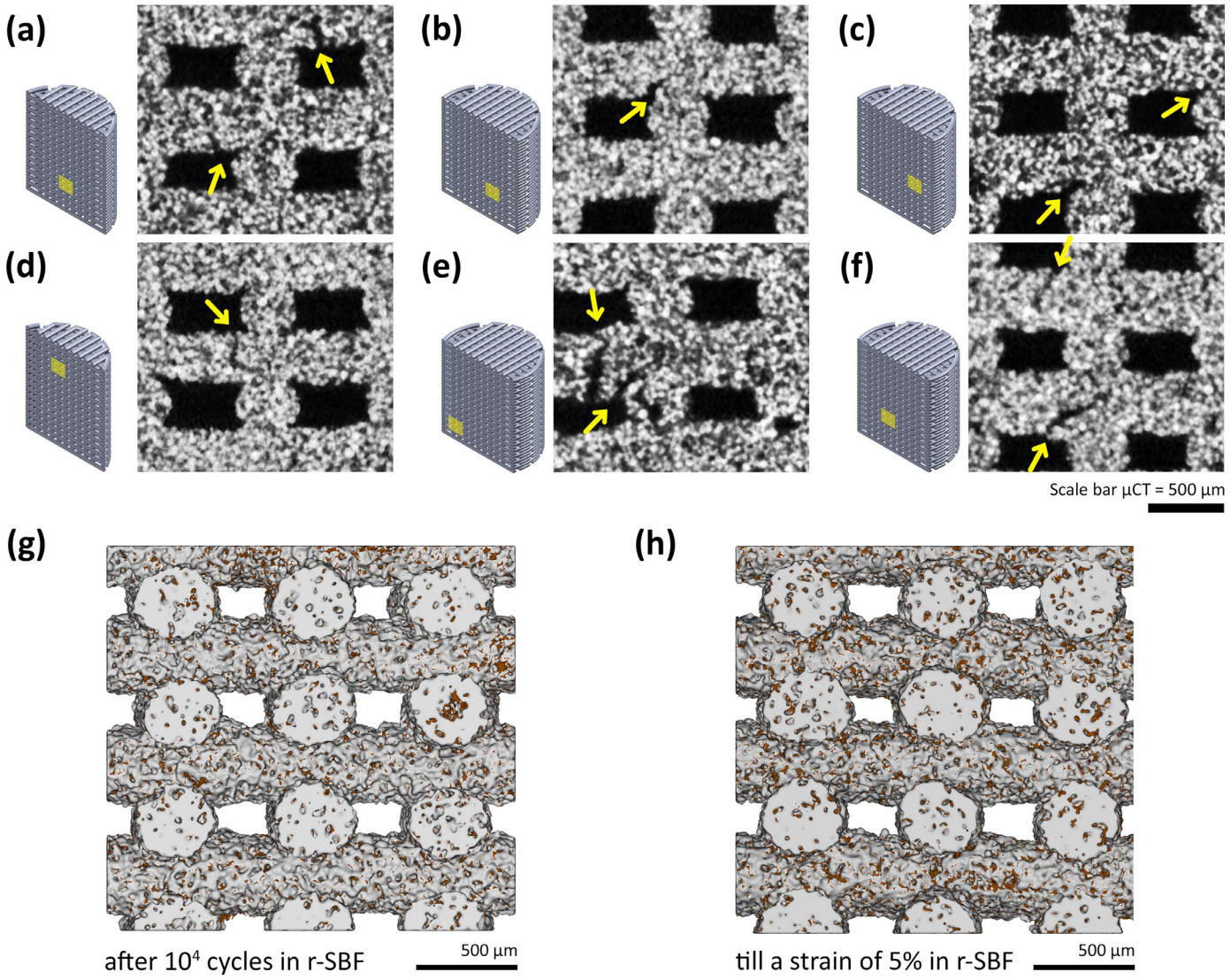

Fig. 7. Fatigue crack distributions across the specimens (a–f) after the corrosion fatigue tests at $0.8\sigma_y$ to a strain of 5 % in r-SBF, visualized by using µCT, and the 3D reconstruction of the specimens (g, h) after the corrosion fatigue tests for 10^4 cycles (to a strain of ~1 %) and to a strain of 5 % at $0.8\sigma_y$. The arrows indicate the cracks at or near the intersections of the struts.

metallic materials [52]. After 3 million cycles of loading at $0.9\sigma_y$ in air, the porous Fe35Mn alloy did not exhibit any cracks until 1.2 % strain accumulation (Fig. S1), demonstrating the inherent fatigue resistance of the AM material. On the other hand, because of *in vitro* biodegradation, the same strain accumulation value was achieved just under the first hundred cycles of loading. During continued corrosion fatigue tests, the strain kept increasing till specimen failure with some fluctuations that could be attributed to the initiation and propagation of cracks across the necks of fused powder particles inside the struts and the formation of corrosion products as evidenced by the SEM images (Fig. 4 and 5) and µCT (Fig. 7).

During the corrosion fatigue tests at $0.6\sigma_y$ to a strain of ~0.5 %, cracks were present only on the periphery of the specimens (Fig. 4b), indicating the sites of crack initiation. Under cyclic loading (*e.g.*, at $0.8\sigma_y$ and $0.9\sigma_y$) up to a strain of 5 %, however, cracks had propagated into the struts (Fig. 4c–f). Crack propagation was observed to occur at the 90° intersection of strut junctions as well (Fig. 7). The characteristic biodegradation fatigue mechanism of the Fe35Mn scaffolds tested in r-SBF and at $0.8\sigma_y$ and $0.9\sigma_y$ are schematically illustrated in Fig. 8. More corrosion products were formed at or near the crack openings during cyclic loading at a higher stress level (Fig. 4f), which can be explained by elevated chemical and electrochemical reactions occurring near or at the crack tip, resulting in the formation of corrosion products [53]. At the center of the scaffolds immersed in r-SBF, cyclic loading at a higher stress level enhanced localized corrosion (Fig. 5e and f). At a lower stress level, the extent of localized corrosion was notably decreased (Fig. 5c and d) and at $0.6\sigma_y$, the localized corrosion was virtually absent (Fig. 5a and b). During the corrosion fatigue tests, at $0.9\sigma_y$, pits of larger sizes appeared on the convex surfaces of fused powder particles in the struts (Fig. 5f), as compared to those in the struts of the specimens subjected to cyclic loading at $0.8\sigma_y$ (Fig. 5d). The local stresses caused by the cyclic loading could break up the corrosion products that would otherwise be compact and dense, as is the case of *in vitro* static biodegradation (Fig. S2) which might trigger the initiation of cracking at the edge of corrosion pits in the center of the scaffolds. Cyclic loading at a higher stress level, corresponding to a higher strain accumulation, may correspond to more fluid exchange through interconnected pores. Consequently, more homogenous biodegradation may occur not only at the concave surfaces of fused powder particles in the struts but also at the convex surfaces, which is beneficial for biodegradable metals.

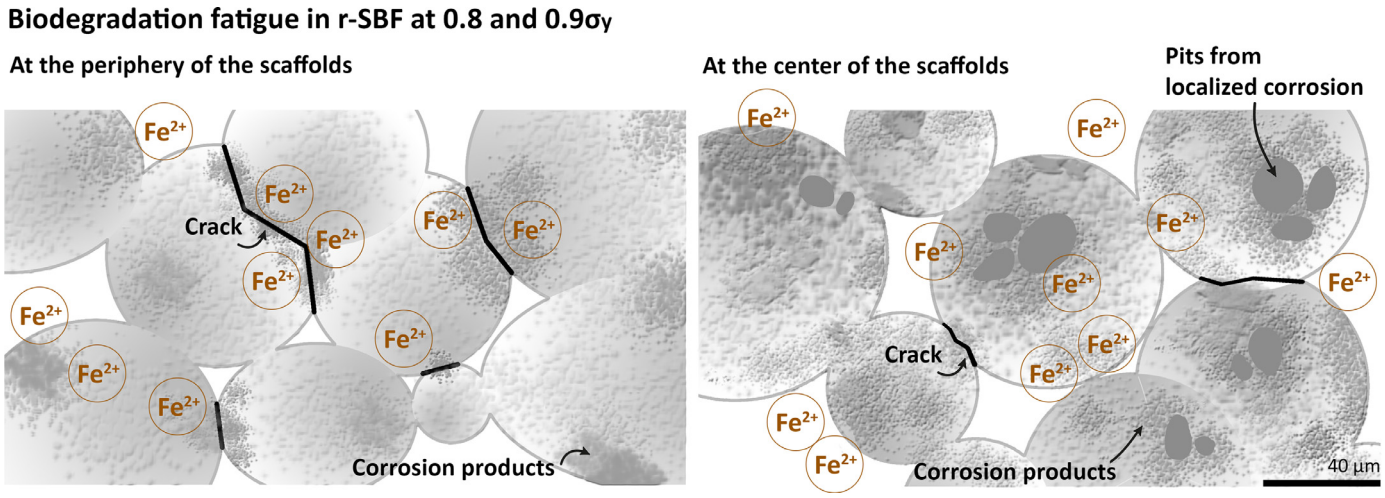

Fig. 8. The corrosion fatigue mechanisms of the porous Fe35Mn alloy scaffolds tested at $0.8\sigma_y$ and $0.9\sigma_y$.

5. Conclusions

We studied, for the first time ever, the fatigue behavior of the architected biodegradable materials made from Fe and Mn elemental powders using extrusion-based AM. The scaffold specimens exhibited high levels of fatigue performance in air and in r-SBF. As expected, cyclic loading accelerated the *in vitro* biodegradation of these scaffolds. Simultaneously, biodegradation reduced the fatigue strength of the specimens (measured at 3 million loading cycles) from 90 % of their yield strength to 60 %. Nevertheless, even in r-SBF, the AM porous Fe35Mn alloy still endured cyclic loading up to 1 million cycles at 90 % of its yield strength. Fatigue cracks preferentially occurred at the necks of fused powder particles in the struts. Crack initiation started on the periphery of the specimens and propagated through the struts. Once a strain of 5 % was reached, cracks were present randomly across the specimen where increased amounts of corrosion products were formed and broken up. Despite the interactions of biodegradation and cyclic loading, the corrosion fatigue resistance of the extrusion-based AM porous Fe35Mn alloy remained at a level promising for its potential use as a trabecular bone-substituting material subjected to compressive loading.

Declaration of competing interest

The authors declare that they have no known competing financial interests or personal relationships that could have appeared to influence the work reported in this paper.

Acknowledgments

Mr. Michel van den Brink at the Department of Process and Energy and Mr. Arjan Thijssen at the Department of Materials, Mechanics, Management & Design, Delft University of Technology, are acknowledged for the ICP-OES analysis and for the µCT analysis, respectively.

Supplementary materials

Supplementary material associated with this article can be found, in the online version, at doi:10.1016/j.actbio.2024.02.024.

References

[1] A. Al Sakkaf, F.S. Januddi, A.H.M. Yusop, H. Nur, Challenges in the use of Fe-based materials for bone scaffolds applications: perspective from in vivo biocorrosion, Mater. Today Commun. 33 (2022) 104564, doi:10.1016/j.mtcomm.2022.104564.
[2] C. Shuai, S. Li, S. Peng, P. Feng, Y. Lai, C. Gao, Biodegradable metallic bone implants, Mater. Chem. Front. 3 (2019) 544–562, doi:10.1039/c8qm00507a.
[3] N.E. Putra, M.A. Leeflang, M. Minneboo, P. Taheri, L.E. Fratila-Apachitei, J.M.C. Mol, J. Zhou, A.A. Zadpoor, Extrusion-based 3D printed biodegradable porous iron, Acta Biomater. 133 (2022) 112617, doi:10.1016/j.actbio.2020.11.022.
[4] D. Carluccio, C. Xu, J. Venezuela, Y. Cao, D. Kent, M. Bermingham, A.G. Demir, B. Previtali, Q. Ye, M. Dargusch, Additively manufactured iron-manganese for biodegradable porous load-bearing bone scaffold applications, Acta Biomater. 103 (2020) 346–360, doi:10.1016/j.actbio.2019.12.018.
[5] N.E. Putra, M.A. Leeflang, P. Taheri, L.E. Fratila-Apachitei, J.M.C. Mol, J. Zhou, A.A. Zadpoor, Extrusion-based 3D printing of ex situ-alloyed highly biodegradable MRI-friendly porous iron-manganese scaffolds, Acta Biomater. 134 (2021) 774–790, doi:10.1016/j.actbio.2021.07.042.
[6] C. Shuai, W. Yang, Y. Yang, H. Pan, C. He, F. Qi, D. Xie, H. Liang, Selective laser melted Fe-Mn bone scaffold: Microstructure, corrosion behavior and cell response, Mater. Res. Express. 7 (2019) 015404, doi:10.1088/2053-1591/ab62f5.
[7] Y. Nie, G. Chen, H. Peng, S. Tang, Z. Zhou, F. Pei, B. Shen, In vitro and 48 weeks in vivo performances of 3D printed porous Fe-30Mn biodegradable scaffolds, Acta Biomater. 121 (2021) 724–740, doi:10.1016/j.actbio.2020.12.028.
[8] T. Kraus, F. Moszner, S. Fischerauer, M. Fiedler, E. Martinelli, J. Eichler, F. Witte, E. Willbold, M. Schinhammer, M. Meischel, P.J. Uggowitzer, J.F. Löffler, A. Weinberg, Biodegradable Fe-based alloys for use in osteosynthesis: Outcome of an in vivo study after 52 weeks, Acta Biomater. 10 (2014) 3346–3353, doi:10.1016/j.actbio.2014.04.007.
[9] M.F. Ulum, A. Arafat, D. Noviana, A.H. Yusop, A.K. Nasution, M.R. Abdul Kadir, H. Hermawan, In vitro and in vivo degradation evaluation of novel iron-bioceramic composites for bone implant applications, Mater. Sci. Eng. C 36 (2014) 336–344, doi:10.1016/j.msec.2013.12.022.
[10] N.E. Putra, M.A. Leeflang, M. Klimopoulou, J. Dong, P. Taheri, Z. Huan, J. Chang, J. Zhou, Extrusion-based 3D printing of biodegradable, osteogenic, paramagnetic, and porous FeMn-akermanite bone substitutes, Acta Biomater. 162 (2023) 182–198, doi:10.1016/j.actbio.2023.03.033.
[11] Y. Li, H. Jahr, J. Zhou, A.A. Zadpoor, Additively manufactured biodegradable porous metals, Acta Biomater. 115 (2020) 29–50, doi:10.1016/j.actbio.2020.08.018.
[12] S. Amin Yavari, S.M. Ahmadi, R. Wauthle, B. Pouran, J. Schrooten, H. Weinans, A.A. Zadpoor, Relationship between unit cell type and porosity and the fatigue behavior of selective laser melted meta-biomaterials, J. Mech. Behav. Biomed. Mater. 43 (2015) 91–100, doi:10.1016/j.jmbbm.2014.12.015.
[13] S.M. Ahmadi, R. Hedayati, Y. Li, K. Lietaert, N. Tümer, A. Fatemi, C.D. Rans, B. Pouran, H. Weinans, A.A. Zadpoor, Fatigue performance of additively manufactured meta-biomaterials: the effects of topology and material type, Acta Biomater. 65 (2018) 292–304, doi:10.1016/j.actbio.2017.11.014.
[14] M.J. Mirzaali, V. Moosabeiki, S.M. Rajaai, J. Zhou, A.A. Zadpoor, Additive manufacturing of biomaterials - design principles and their implementation, Materials (Basel) 15 (2022) 5457, doi:10.3390/ma15155457.
[15] Y. Li, K. Lietaert, W. Li, X.Y. Zhang, M.A. Leeflang, J. Zhou, A.A. Zadpoor, Corrosion fatigue behavior of additively manufactured biodegradable porous iron, Corros. Sci. 156 (2019) 106–116, doi:10.1016/j.corsci.2019.05.003.

[16] Y. Li, H. Jahr, X.Y. Zhang, M.A. Leeflang, W. Li, B. Pouran, F.D. Tichelaar, H. Weinans, J. Zhou, A.A. Zadpoor, Biodegradation-affected fatigue behavior of additively manufactured porous magnesium, Addit. Manuf. 28 (2019) 299–311, doi:10.1016/j.addma.2019.05.013.
[17] Y. Li, W. Li, F.S.L. Bobbert, K. Lietaert, J.H. Dong, M.A. Leeflang, J. Zhou, A.A. Zadpoor, Corrosion fatigue behavior of additively manufactured biodegradable porous zinc, Acta Biomater. 106 (2020) 439–449, doi:10.1016/j.actbio.2020.02.001.
[18] D. Zhao, C. Han, B. Peng, T. Cheng, J. Fan, L. Yang, L. Chen, Q. Wei, Corrosion fatigue behavior and anti-fatigue mechanisms of an additively manufactured biodegradable zinc-magnesium gyroid scaffold, Acta Biomater. 153 (2022) 614–629, doi:10.1016/j.actbio.2022.09.047.
[19] A. Oyane, H.M. Kim, T. Furuya, T. Kokubo, T. Miyazaki, T. Nakamura, Preparation and assessment of revised simulated body fluids, J. Biomed. Mater. Res. - Part A 65 (2003) 188–195, doi:10.1002/jbm.a.10482.
[20] A. Berner, M.A. Woodruff, C.X.F. Lam, M.T. Arafat, S. Saifzadeh, R. Steck, J. Ren, M. Nerlich, A.K. Ekaputra, I. Gibson, D.W. Hutmacher, Effects of scaffold architecture on cranial bone healing, Int. J. Oral Maxillofac. Surg. 43 (2014) 506–513, doi:10.1016/j.ijom.2013.05.008.
[21] M. Paris, A. Götz, I. Hettrich, C.M. Bidan, J.W.C. Dunlop, H. Razi, I. Zizak, D.W. Hutmacher, P. Fratzl, G.N. Duda, W. Wagermaier, A. Cipitria, Scaffold curvature-mediated novel biomineralization process originates a continuous soft tissue-to-bone interface, Acta Biomater. 60 (2017) 64–80, doi:10.1016/j.actbio.2017.07.029.
[22] H. Hermawan, H. Alamdari, D. Mantovani, D. Dubé, Iron-manganese: new class of metallic degradable biomaterials prepared by powder metallurgy, Powder Metall. 51 (2008) 38–45, doi:10.1179/174329008×284868.
[23] R. Domander, A.A. Felder, M. Doube, D. Schmidt, BoneJ2 - refactoring established research software, Wellcome Open Res. (2021) 1–21.
[24] R. Hedayati, S.M. Ahmadi, K. Lietaert, N. Tümer, Y. Li, S. Amin Yavari, A.A. Zadpoor, Fatigue and quasi-static mechanical behavior of bio-degradable porous biomaterials based on magnesium alloys, J. Biomed. Mater. Res. - Part A 106 (2018) 1798–1811, doi:10.1002/jbm.a.36380.
[25] D.L. Kopperdahl, T.M. Keaveny, Yield strain behavior of trabecular bone, J. Biomech. 31 (1998) 601–608, doi:10.1016/S0021-9290(98)00057-8.
[26] E.F. Morgan, T.M. Keaveny, Dependence of yield strain of human trabecular bone on anatomic site, J. Biomech. 34 (2001) 569–577, doi:10.1016/S0021-9290(01)00011-2.
[27] N. Sanaei, A. Fatemi, Defects in additive manufactured metals and their effect on fatigue performance: a state-of-the-art review, Prog. Mater. Sci. 117 (2021) 100724, doi:10.1016/j.pmatsci.2020.100724.
[28] A.Y. Al-Maharma, S.P. Patil, B. Markert, Effects of porosity on the mechanical properties of additively manufactured components: a critical review, Mater. Res. Express. 7 (2020) 122001, doi:10.1088/2053-1591/abcc5d.
[29] K. Slámečka, A. Kashimbetova, J. Pokluda, T. Zikmund, J. Kaiser, E.B. Montufar, L. Čelko, Fatigue behaviour of titanium scaffolds with hierarchical porosity produced by material extrusion additive manufacturing, Mater. Des. 225 (2023) 111453, doi:10.1016/j.matdes.2022.111453.
[30] H.M.A. Kolken, A.F. Garcia, A. Du Plessis, C. Rans, M.J. Mirzaali, A.A. Zadpoor, Fatigue performance of auxetic meta-biomaterials, Acta Biomater. 126 (2021) 511–523, doi:10.1016/j.actbio.2021.03.015.
[31] A.R. Stern, D.P. Nicolella, Measurement and estimation of osteocyte mechanical strain, Bone 54 (2013) 191–195, doi:10.1016/j.bone.2013.01.037.
[32] A.A. Zadpoor, Bone tissue regeneration: the role of scaffold geometry, Biomater. Sci. 3 (2015) 231–245, doi:10.1039/c4bm00291a.
[33] H. Mohammadi, M. Sepantafar, N. Muhamad, A. Bakar Sulong, How does scaffold porosity conduct bone tissue regeneration? Adv. Eng. Mater. 23 (2021) 1–19, doi:10.1002/adem.202100463.
[34] N. Abbasi, S. Hamlet, R.M. Love, N.T. Nguyen, Porous scaffolds for bone regeneration, J. Sci. Adv. Mater. Devices 5 (2020) 1–9, doi:10.1016/j.jsamd.2020.01.007.
[35] I. Buj-Corral, A. Domínguez-Fernández, A. Gómez-Gejo, Effect of printing parameters on dimensional error and surface roughness obtained in direct ink writing (DIW) processes, Materials (Basel). 13 (2020) 2157. https://doi.org/10.3390/ma13092157.
[36] K. Solberg, S. Guan, S.M.J. Razavi, T. Welo, K.C. Chan, F. Berto, Fatigue of additively manufactured 316L stainless steel: the influence of porosity and surface roughness, Fatigue Fract. Eng. Mater. Struct. 42 (2019) 2043–2052, doi:10.1111/ffe.13077.
[37] B. Vayssette, N. Saintier, C. Brugger, M. El May, Surface roughness effect of SLM and EBM Ti-6Al-4V on multiaxial high cycle fatigue, Theor. Appl. Fract. Mech. 108 (2020) 102581, doi:10.1016/j.tafmec.2020.102581.
[38] J. Gockel, L. Sheridan, B. Koerper, B. Whip, The influence of additive manufacturing processing parameters on surface roughness and fatigue life, Int. J. Fatigue 124 (2019) 380–388, doi:10.1016/j.ijfatigue.2019.03.025.
[39] A. Rodriguez-Contreras, D. Guadarrama Bello, A. Nanci, Surface nanoporosity has a greater influence on osteogenic and bacterial cell adhesion than crystallinity and wettability, Appl. Surf. Sci. 445 (2018) 255–261, doi:10.1016/j.apsusc.2018.03.150.
[40] R.A. Gittens, T. McLachlan, R. Olivares-Navarrete, Y. Cai, S. Berner, R. Tannenbaum, Z. Schwartz, K.H. Sandhage, B.D. Boyan, The effects of combined micron-/submicron-scale surface roughness and nanoscale features on cell proliferation and differentiation, Biomaterials 32 (2011) 3395–3403, doi:10.1016/j.biomaterials.2011.01.029.
[41] I. Georgakopoulos-Soares, E.L. Papazoglou, P. Karmiris-Obratański, N.E. Karkalos, A.P. Markopoulos, Surface antibacterial properties enhanced through engineered textures and surface roughness: a review, Colloids Surf. B Biointerfaces 231 (2023) 113584, doi:10.1016/j.colsurfb.2023.113584.
[42] Y. Li, H. Jahr, K. Lietaert, P. Pavanram, A. Yilmaz, L.I. Fockaert, M.A. Leeflang, B. Pouran, Y. Gonzalez-Garcia, H. Weinans, J.M.C. Mol, J. Zhou, A.A. Zadpoor, Additively manufactured biodegradable porous iron, Acta Biomater. 77 (2018) 380–393, doi:10.1016/j.actbio.2018.07.011.
[43] F. Li, J. Li, H. Kou, L. Zhou, Porous Ti6Al4V alloys with enhanced normalized fatigue strength for biomedical applications, Mater. Sci. Eng. C 60 (2016) 485–488, doi:10.1016/j.msec.2015.11.074.
[44] B.R. Merk, S.H. Stern, S. Cordes, E.P. Lautenschlager, A fatigue life analysis of small fragment screws, J. Orthop. Trauma. 15 (2001) 494–499, doi:10.1097/00005131-200109000-00006.
[45] S.M. Hou, J.L. Wang, J. Lin, Mechanical strength, fatigue life, and failure analysis of two prototypes and five conventional tibial locking screws, J. Orthop. Trauma. 16 (2002) 701–708, doi:10.1097/00005131-200211000-00004.
[46] L. Rapillard, M. Charlebois, P.K. Zysset, Compressive fatigue behavior of human vertebral trabecular bone, J. Biomech. 39 (2006) 2133–2139, doi:10.1016/j.jbiomech.2005.04.033.
[47] M. Silva, E.F. Shepherd, W.O. Jackson, F.J. Dorey, T.P. Schmalzried, Average patient walking activity approaches 2 million cycles per year: pedometers underrecord walking activity, J. Arthroplasty 17 (2002) 693–697, doi:10.1054/arth.2002.32699.
[48] V.S. Nikolaou, N. Efstathopoulos, G. Kontakis, N.K. Kanakaris, P.V. Giannoudis, The influence of osteoporosis in femoral fracture healing time, Injury 40 (2009) 663–668, doi:10.1016/j.injury.2008.10.035.
[49] R. Hedayati, S. Janbaz, M. Sadighi, M. Mohammadi-Aghdam, A.A. Zadpoor, How does tissue regeneration influence the mechanical behavior of additively manufactured porous biomaterials? J. Mech. Behav. Biomed. Mater. 65 (2017) 831–841, doi:10.1016/j.jmbbm.2016.10.003.
[50] Y.J. Liu, H.L. Wang, S.J. Li, S.G. Wang, W.J. Wang, W.T. Hou, Y.L. Hao, R. Yang, L.C. Zhang, Compressive and fatigue behavior of beta-type titanium porous structures fabricated by electron beam melting, Acta Mater. 126 (2017) 58–66, doi:10.1016/j.actamat.2016.12.052.
[51] S.J. Li, L.E. Murr, X.Y. Cheng, Z.B. Zhang, Y.L. Hao, R. Yang, F. Medina, R.B. Wicker, Compression fatigue behavior of Ti-6Al-4V mesh arrays fabricated by electron beam melting, Acta Mater. 60 (2012) 793–802, doi:10.1016/j.actamat.2011.10.051.
[52] L. Yang, C. Yan, W. Cao, Z. Liu, B. Song, S. Wen, C. Zhang, Y. Shi, S. Yang, Compression–compression fatigue behaviour of gyroid-type triply periodic minimal surface porous structures fabricated by selective laser melting, Acta Mater. 181 (2019) 49–66, doi:10.1016/j.actamat.2019.09.042.
[53] L.G. Bland, J.S.W. Locke, Chemical and electrochemical conditions within stress corrosion and corrosion fatigue cracks, NPJ Mater. Degrad. 1 (2017) 1–8, doi:10.1038/s41529-017-0015-0.